C. R. Mecanique 346 (2018) 919–931

Contents lists available at ScienceDirect

Comptes Rendus Mecanique

www.sciencedirect.com

Jet noise modelling and control / Modélisation et contrôle du bruit de jet

Acceleration and wall pressure fluctuations generated by an incompressible jet in installed configuration

Matteo Mancinelli [a,*], Roberto Camussi [b]

[a] Institut Pprime – CNRS, Université de Poitiers, ENSMA – Département Fluides, Thermique et Combustion, 11, boulevard Marie-et-Pierre-Curie, 86962 Chasseneuil-du-Poitou, Poitiers, France
[b] Università degli Studi Roma Tre, Dipartimento di Ingegneria, Via della Vasca Navale 79, 00146 Rome, Italy

ARTICLE INFO

Article history:
Received 24 May 2017
Accepted 1 February 2018
Available online 2 August 2018

Keywords:
Fluid mechanics
Jets
Aeroacoustics

ABSTRACT

In this work, the cross-statistics of acceleration and wall pressure fluctuations generated by an incompressible jet interacting with a tangential flat-plate are presented. The results are derived from an experimental test campaign on a laboratory-scale model involving simultaneous velocity and wall pressure measurements. The pressure footprint of the jet on the surface was measured through a cavity-mounted microphone array, whereas pointwise velocity measurements were carried out by a hot wire anemometer. The time derivative of the velocity signal has been taken as an estimation of the local acceleration of the jet. The multivariate statistics between acceleration and wall pressure are achieved through cross-correlations and cross-spectra, highlighting that the causality relation is more significant in the potential core where the Kelvin–Helmholtz instability is dominant. The application of a conditional sampling procedure based on wavelet transform allowed us to educe the acceleration flow structures related to the energetic wall-pressure events. The analysis revealed that, unlike the velocity, the acceleration signatures were detected only for positions where the jet had not yet impinged on the plate, their shape being related to a convected wavepacket structure.

1. Introduction

The increasing size of aircraft engines is bringing about strong concerns for their conventional under-wing installation due to the interaction between the exhausting jet and the airframe components. As pointed out by Huber et al. [1,2], the increase of the radiated acoustic emissions due to the jet–wing interaction can jeopardize the noise breakdown achieved by the jet velocity reduction consequent to the increase of the By-Pass Ratio (BPR) in the new engine models. On the other hand, the pressure fluctuations generated by the jet impinging on the fuselage play a fundamental role in terms of panels structural strength and generation of interior noise. Indeed, the jet impact on the fuselage induces panel stress and vibrations, these vibrations being partially re-emitted in the aeroacoustic field and partially transmitted to the aircraft cockpit, causing passengers' annoyance. Hence, manufacturers are investing in research to develop appropriate technologies to mitigate the installation effects in the future aircraft configurations. As a consequence, a deeper insight on the complex mechanism underlying the jet–surface interaction is needed.

* Corresponding author.
E-mail addresses: matteo.mancinelli@univ-poitiers.fr (M. Mancinelli), roberto.camussi@uniroma3.it (R. Camussi).

https://doi.org/10.1016/j.crme.2018.07.008
1631-0721/

Many studies in the literature were devoted to the investigation of the effect of a surface on the emitted far-field noise (see, e.g., Papamoschou & Mayoral [3] and Podboy [4]). The shielding/scattering effect of a flat-plate tangential to the nozzle axis of a compressible jet was studied by Cavalieri et al. [5], where the acoustic emissions of the jet were computed through a wavepacket source model. More recently, Piantanida et al. [6] highlighted that a strong deformation of the aerodynamic field is expected when the mutual distance between the jet and the surface becomes of the order of the nozzle diameter, the jet–surface interaction being consequently stronger. Hence, the investigation of the incident pressure field in addition to the scattered one can provide a better understanding of the interaction phenomena between the jet and the surface [7]. Indeed, as pointed out by Di Marco et al. [8], the characterization of the spectral content of the wall pressure fluctuations is essential to develop appropriate tools for noise prediction and verification of the structural strength of the panels.

The discussion above motivated the authors to carry out a series of experimental tests on a laboratory-scale model to characterise the installation effects of a flat plate tangential to an incompressible jet [9]. The jet–surface interaction was mainly studied in terms of statistical and spectral features of the wall-pressure field, laying the foundations for the modelling of the wall-pressure fluctuations. The jet flow conditions as well as the geometry were significantly simplified with respect to the real industrial problem. Nevertheless, the novelty of the approach offered the basis for an improved physical understanding of the jet–plate interaction phenomena. Furthermore, as reported by Di Marco et al. [8], the weak dependence of the wall pressure features on Mach and Reynolds numbers of the flow suggested that the outcome obtained in incompressible conditions could be likely extended to jet–surface configurations with higher velocities. Such aspect encouraged the authors to extend the previous work in Mancinelli et al. [10,11], where simultaneous velocity and wall pressure measurements were carried out on the same configuration. The aerodynamic field was characterised through pointwise single-component hot-wire (HW) anemometer measurements, whereas the streamwise evolution of the wall-pressure fluctuation field was measured by a cavity-mounted microphone array. The plate effect on the velocity field was addressed as well as the multi-variate statistics between velocity and wall-pressure fields were provided. The conditioned statistics were also achieved through the application of a wavelet-based conditional sampling procedure that revealed the velocity and wall-pressure signatures underlying the interaction phenomena between the jet and the flat-plate.

In the present work, the investigation on the same installed configuration is further extended, performing a cross-statistical and conditional sampling analysis between the wall-pressure and the acceleration fields. A preliminary analysis of the acceleration field in free-jet conditions is also provided. To the best of the authors' knowledge, this represents the first attempt to characterise experimentally the acceleration field of a jet. The main motivation of such an approach lies in the Euler's equation, where the pressure gradient, i.e. a term related to vorticity and entropy fields as well as strictly associated with noise emissions ([12] and [13]), is a function of the acceleration. According to Camussi & Grizzi [14], the time derivative of the velocity signal has been taken as an estimation of the local acceleration of the jet, the computation of the convective term related to the spatial velocity gradient through parallel double-component HW or PIV measurements being a task for future applications. The cross-statistics between acceleration and wall pressure fluctuations are provided in both the time and frequency domains. A wavelet-based cross-conditioning technique permitted to educe the coherent acceleration structures associated with the energetic wall pressure events. The outcome was compared with the results obtained in Mancinelli et al. [10,11] using the velocity instead of the acceleration.

The paper is organised as follows. In §2, the experimental set-up is briefly described, and details about the initial state of the jet flow are given, whereas in §3 the conditional sampling procedure based on wavelet transform is summarised. §4 is devoted to the presentation of the main results concerning the characterisation of the acceleration field, the multi-variate and the conditioned statistics between acceleration and wall pressure. Final remarks are addressed in §5.

2. Experimental set-up

The experiments were performed in the Aerodynamic and Thermo-fluid dynamic Laboratory of the Department of Engineering of University Roma Tre. The facility reproduces the one presented in [15] and is briefly described in the following. The flow is generated by a centrifugal blower and is guided into a wide-angle diffuser, then it issues in a plenum chamber where honeycomb panel and turbulence grids are installed. The fluid finally flows into a quiescent ambient through a convergent nozzle with a diameter $D = 52\,\text{mm}$. A sketch of the facility is represented in Fig. 1.

The experiments were carried out at a nominal jet velocity $U_j = 42\,\text{m}\cdot\text{s}^{-1}$, to which correspond Mach and nozzle diameter-based Reynolds numbers of 0.12 and $1.5 \cdot 10^5$, respectively, which classify the jet as a moderate Reynolds number jet [16]. The mean velocity and turbulence intensity profiles close to the nozzle exhaust at the streamwise position $x/D = 1$ are shown in Fig. 2. As outlined by Zaman [17], the laminar Blasius-like shape of the mean velocity profile is associated with a high turbulence intensity peak of the order of 10%. Such feature implies that the jet was in a transitional highly disturbed initial state, or nominally turbulent according to Bogey et al. [16,18]. For a more detailed description of the facility and for the characterization of the jet flow, the reader can refer to Di Marco et al. [9].

Simultaneous velocity and wall pressure measurements were carried out in an installed configuration. A flat plate was placed tangentially to the jet at different radial distances H from the nozzle axis, spanning a range from $1\,D$ to $2.5\,D$ with a step of $0.5\,D$. The area of interest was divided into five measurement stations, each station being constituted by five measurement locations along the streamwise direction, in order to cover the range $x/D = [1, 25]$. The streamwise evolution of the wall pressure fluctuation field was provided by cavity-mounted 5-microphone array measurements, while the velocity field was characterised by hot-wire anemometer measurements, the HW being moved along the z-direction orthogonal to

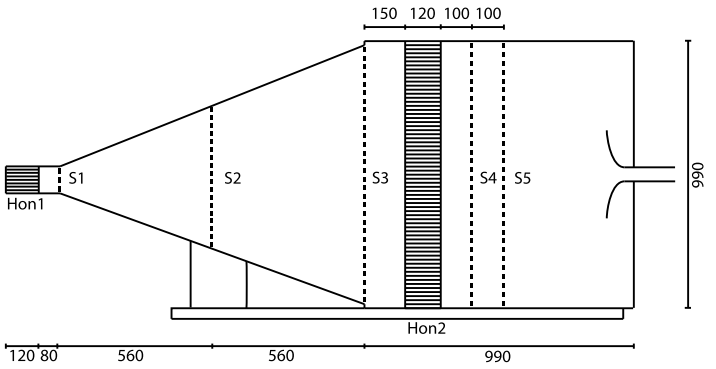

Fig. 1. Representation of the jet facility. Hon# and S# indicate the honeycomb panel and the turbulence screens, respectively.

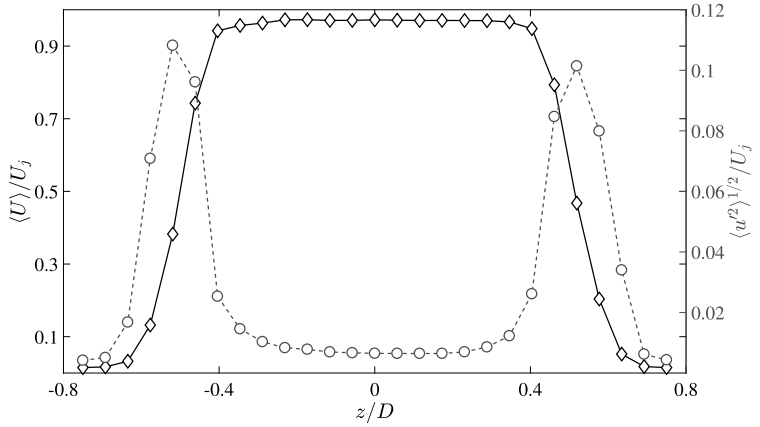

Fig. 2. Mean velocity and turbulence intensity profiles at the streamwise position $x/D = 1$: ◇ refer to the mean velocity, ○ refer to the turbulence level.

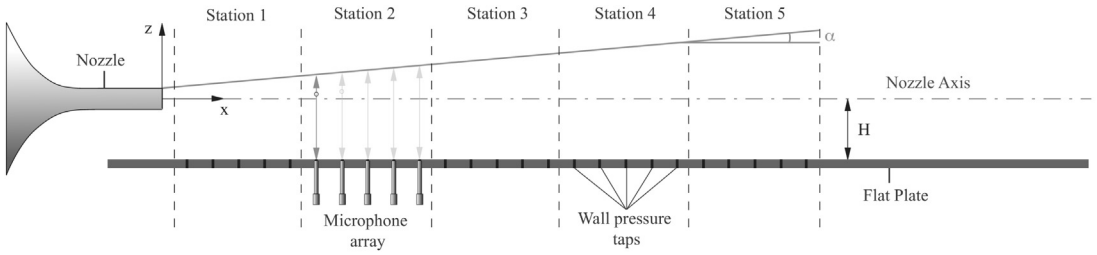

Fig. 3. Scheme of the jet–plate installation and of the instrumentation disposition.

the plate for different axial distances x. The minimum transverse distance between the HW and the surface is referred hereinafter as ζ, its value being equal to 5 mm. The wall pressure measurements were performed by Microtech Gefell M360 microphones, whereas the single-component hot-wire probe Dantec 55P11 was connected to a Constant Temperature Anemometer AN1003 Lab-System. Data were acquired by a digital scope Yokogawa DL708E at a sampling frequency of 50 kHz for an acquisition time of 20 s. A scheme of the jet–plate installation and the instrumentation disposition as well as of the reference system adopted is depicted in Fig. 3 (for more information, the reader can refer to Mancinelli et al. [10,11]).

3. Wavelet-based cross-conditioning procedure

The eduction of the acceleration flow structures was achieved by the application of a wavelet conditioning procedure based on the detection of energetic pressure events. The main concepts of the procedure are discussed in Camussi & Guj [19], whereas, for a comprehensive review on wavelet transform and its application, the reader may refer to Torrence & Compo [20] and Farge [21].

The Continuous Wavelet Transform (CWT) of a given time function $f(t)$ consists of a projection over a basis of compact support functions obtained by dilations and translations of the mother wavelet $\Psi(t)$. The mother wavelet is localized in both

the physical and transformed spaces, the resulting wavelet coefficients being a function of the time t and of the scale s, which is inversely proportional to the frequency [22]. According to Meneveau [23], the CWT of a time signal can be defined as follows:

$$w(s,t) = C_{\psi}^{-1/2} s^{-1/2} \int_{-\infty}^{+\infty} f(\tau)\, \Psi^* \left(\frac{t-\tau}{s} \right) \mathrm{d}\tau \tag{1}$$

where $C_{\psi}^{-1/2}$ is a constant allowing one to take into account the mean value of $\Psi(t)$ and $\Psi^* \left(\frac{t-\tau}{s}\right)$ is the complex conjugate of the dilated and translated $\Psi(t)$.

In the present work, the CWT was computed using a Mexican Hat kernel by means of the *Matlab*© wavelet toolbox. As previously outlined by Farge [21] and Camussi et al. [24], the independence of the educed signatures from the mother wavelet adopted was verified, such a result being not reported herein for the sake of brevity. The CWT was applied to time signals in order to select a set of reference times of high-energy events. Indeed, the extraction of the coherent signatures is based on an energetic criterion. As pointed out by Farge [21], the normalized energy content of a time signal at the scale s and the instant t can be evaluated computing the Local Intermittency Measure (LIM):

$$LIM(s,t) = \frac{w^2(s,t)}{\langle w^2(s,t) \rangle_t} \tag{2}$$

where the symbol $\langle\rangle_t$ denotes a time average. The coherent structures identification procedure is based on the idea that the passage of a high-energy flow structure of a characteristic size s_i at the instant t_k, should induce a burst in the LIM at the corresponding time-scale location [25]. The LIM can be thresholded, fixing a proper trigger level T, to select relative maxima that satisfy the condition $LIM(s_i, t_k) > T$. Once reference time instants t_k^* fulfilling the triggering condition are selected, a set of signal segments centred in the time instants t_k^* is extracted, and an ensemble average of the set is performed, revealing the time signatures hidden in the original signal. The independence of the educed signatures from the selected threshold level T has been verified (see also Camussi et al. [26,24] and Mancinelli et al. [11]).

In the present approach, the cross-conditioning procedure is based on the selection of events from the wall-pressure time series $p(t)$ and the conditional average of the acceleration signal segments $a(t)$, as formally reported in the following:

$$\langle a \mid p \rangle = \frac{1}{N_e} \sum_{k=1}^{N_e} a\left(t_k^* - \Delta t, t_k^* + \Delta t\right) \tag{3}$$

where N_e is the number of events corresponding to the condition $LIM(s_i, t_k) > T$ and Δt is a proper time window dependent on the estimated persistence of the effect of the detected singularity (see Mancinelli et al. [10,11]). The educed signatures $\langle a \rangle$ represent the shape of the coherent content embedded in the chaotic time signal $a(t)$ related to energetic events in the signal $p(t)$.

4. Results

4.1. Characterization of the acceleration field

In this section, a statistical and spectral characterization of the acceleration in the jet plume is provided in both free and installed configurations. For an analogous analysis of the velocity field, the reader may refer to Di Marco et al. [9] and Mancinelli et al. [10,11]. As outlined in §1, the acceleration has been estimated as the time derivative of the velocity signal measured by the HW anemometer. The time derivative was computed by means of a Finite Difference Method with a forward scheme. The kth acceleration element is evaluated according to the following formula:

$$a_k = \left. \frac{\partial u}{\partial t} \right|_k = \frac{u_{k+1} - u_k}{T_s} \tag{4}$$

where u is the axial velocity and T_s is the sampling time. The accuracy of the acceleration estimation performed was checked by comparing the results obtained with the forward scheme against the ones obtained using a higher-order centred scheme. No significant discrepancies were detected between the two computation schemes, such an outcome being not reported herein for the sake of conciseness.

4.1.1. Free-jet conditions

Fig. 4 shows the axial evolution along the nozzle axis of the acceleration statistical moments up to the fourth order. The mean and fluctuating accelerations were normalized, dividing by a characteristic flow acceleration estimated by the ratio between the square jet velocity U_j^2 and the nozzle diameter D. As expected, the mean acceleration is zero for all the axial positions. The standard deviation value remains almost zero for small axial positions, then it increases, reaching a maximum

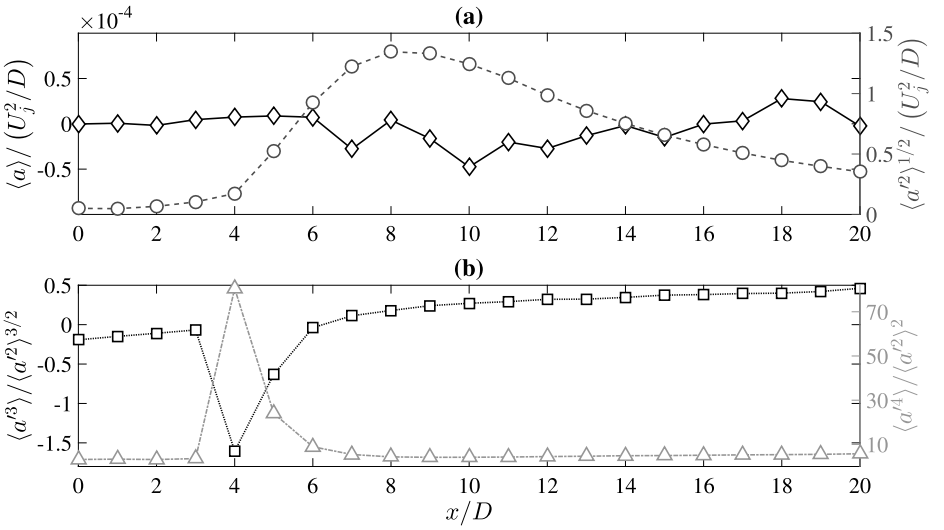

Fig. 4. Streamwise evolution along the nozzle axis of the acceleration statistical moments in free-jet conditions. (a) Mean and fluctuating acceleration: ◇ refer to the mean acceleration, ○ to the standard deviation. (b) skewness and flatness factors: □ refer to the skewness factor, △ to kurtosis.

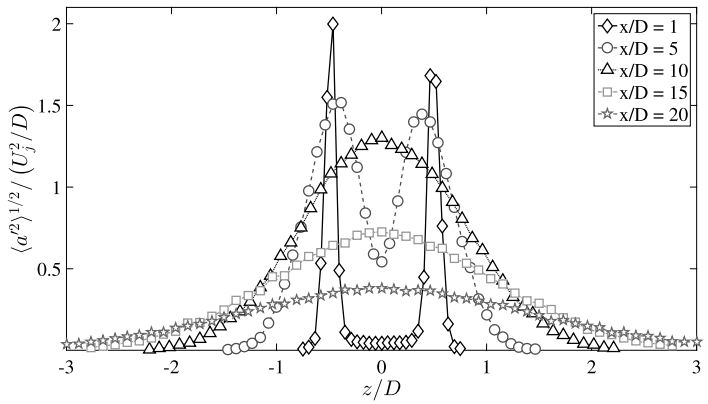

Fig. 5. Profiles along the z-direction of the acceleration standard deviation at different axial distances in free-jet conditions.

downstream of the potential core end (i.e. $x/D \approx 5$–6 according to previous results presented in [9]). On the contrary, the skewness factor shows negative values for small stream-wise locations and positive ones for large axial distances, whereas the kurtosis exhibits values larger than 3 for all the axial positions considered. Both the third- and fourth-order statistical moments exhibit a singularity for the axial position $x/D = 4$, i.e. just before the potential core end.

The profiles of the acceleration standard deviation along the z-direction for different axial distances x are reported in Fig. 5. It is observed that, in the potential core, the fluctuation intensity is small in the central part of the jet and larger in the proximity of the mixing layers. It has to be underlined that, unlike the velocity profile shown in Fig. 2, a slight asymmetry of the fluctuating acceleration profile is detected for $x/D = 1$. Such a behaviour could be due to a larger statistical uncertainty in the computation of the acceleration standard deviation, this feature being a consequence of the time derivative operation. For axial positions downstream of the potential core end, a Gaussian-like profile shape appears. It has to be pointed out that the acceleration standard deviation profiles exhibit a shape similar to the canonical one of the turbulence intensity profiles [9]. The resemblance between the fluctuating acceleration and velocity profiles could be explained by considering the mathematical process reported in the following. The variance of the acceleration can be written as:

$$\begin{aligned} \langle a'^2 \rangle &= \langle \frac{\partial u'}{\partial t} \frac{\partial u'}{\partial t} \rangle = \langle \left(\frac{\partial u'}{\partial t} \right)^2 \rangle \approx \langle \left(\frac{\Delta u'}{\Delta t} \right)^2 \rangle = \frac{1}{T_s^2} \langle \left(\Delta u' \right)^2 \rangle = \frac{1}{T_s^2 \left(N_s - 1 \right)} \sum_{k=1}^{N_s - 1} \left(\Delta u'_k \right)^2 \\ &= \frac{1}{T_s^2 \left(N_s - 1 \right)} \sum_{k=1}^{N_s - 1} \left(u'_{k+1} - u'_k \right)^2 = \frac{1}{T_s^2 \left(N_s - 1 \right)} \sum_{k=1}^{N_s - 1} \left(u'^2_{k+1} - 2 u'_k u'_{k+1} + u'^2_k \right) \end{aligned} \tag{5}$$

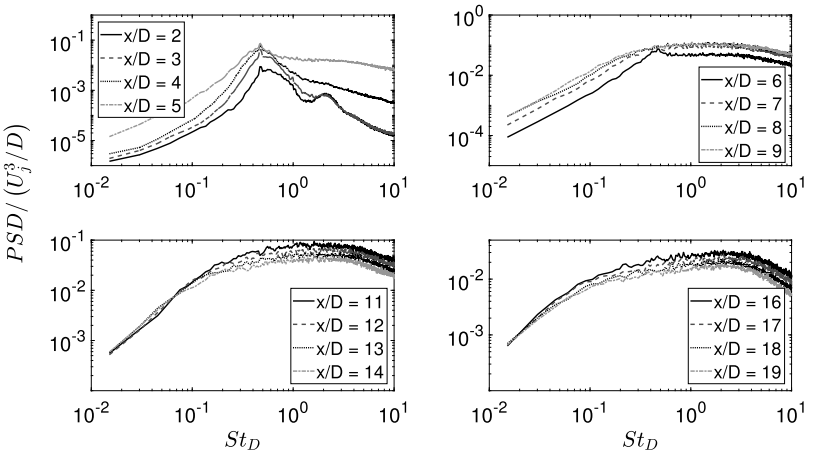

Fig. 6. Streamwise evolution along the nozzle axis of the dimensionless acceleration spectra in free-jet conditions.

If the hypothesis $\sum_k u'^2_{k+1} \approx \sum_k u'^2_k$ is assumed, the acceleration variance can be finally defined as:

$$\begin{aligned} \langle a'^2 \rangle &= \langle \left(\frac{\partial u'}{\partial t} \right)^2 \rangle \approx \frac{2}{T_s^2 (N_s - 1)} \left(\sum_{k=1}^{N_s-1} u'^2_{k+1} - \sum_{k=1}^{N_s-1} u'_k u'_{k+1} \right) \\ &\approx \frac{2}{T_s^2} \langle u'^2 \rangle - \frac{2}{T_s^2 (N_s - 1)} \sum_{k=1}^{N_s-1} u'_k u'_{k+1} = \frac{2}{T_s^2} \left(R_{uu}(0) - R_{uu}(T_s) \right) \end{aligned} \tag{6}$$

where N_s and $R_{uu}(\tau)$ are the number of samples and the auto-correlation function of the velocity signal, respectively. The development reported above shows that the acceleration fluctuation intensity is related to the difference between the velocity auto-correlation at zero and first time-lags, i.e. the de-correlation speed of the velocity signal. Hence, the acceleration fluctuation amplitude is larger when the velocity de-correlation is faster, that is when the velocity signal has a stronger stochastic nature, i.e. where turbulence and non-linear effects are more significant as in the shear layer or downstream of the potential core end. Such a behaviour corroborates the relevance of acceleration as an interesting parameter to look at in jet flow analysis.

The streamwise evolution of the acceleration spectral content is reported in Fig. 6, which shows the dimensionless Power Spectral Densities (PSDs) along the nozzle axis. The PSDs were normalized by dividing by a characteristic flow time scale, i.e. D/U_j, and by dividing by the square of the ratio U_j^2/D, the resulting scaling parameter being U_j^3/D. Spectra are plotted against a Strouhal number based on the jet velocity and the nozzle diameter. The spectra show a steep ascent at low frequencies with a more significant energy content in the high-frequency range. Such a behaviour is related to the time derivative operation that implies in the Fourier domain the multiplication of the velocity signal by the quantity $i\omega$. The effect of this operation is the enhancement of the energy content at middle/high frequencies, where, according to previous results on the spectral characterization of the velocity field presented by the authors in [9], the Kelvin–Helmholtz instability mode was found to be dominant for axial positions within the potential core. This assertion is supported by the emergence of an energy peak for a Strouhal number ≈ 0.47 for $x/D \leq 6$, such a behaviour being the signature of the roll-up of the shear layer. The spectral characterization of the acceleration field is further provided in Fig. 7, which shows the normalized PSD map along the z-direction at different axial distances. It is observed that for small axial distances within the potential core the spectral energy is mainly concentrated in the mixing layers of the jet. A significant tonal component clearly appears for the typical Strouhal number associated with the Kelvin–Helmholtz instability for all the crosswise positions. As the axial distance increases, the energy content reduces and spreads on a wider range of transverse positions z.

4.1.2. Plate effect on the acceleration field

Fig. 8 shows the contour maps of the dimensionless standard deviation of the acceleration field in the plane x–z. It is observed that the acceleration fluctuation intensity is almost zero in the potential core region and is larger in the mixing layers. As already underlined for the mean and fluctuating velocity fields [10,11], the effect of the plate is to modify the axisymmetry of the jet. The Coanda effect induces the bending of the jet over the surface, such a behaviour being more significant for closer jet–plate configurations.

The characterization of the acceleration field in the installed configuration is further provided by the contour maps in the plane x–z of the third- and fourth-order statistical moments shown in Figs. 9 and 10, respectively. The skewness factor is close to 0 in the jet plume, with the exception of the inner and outer shear layers, where negative and positive values are found, respectively. The positive values in the outer shear layers are ascribed to the entrainment effect of the jet that

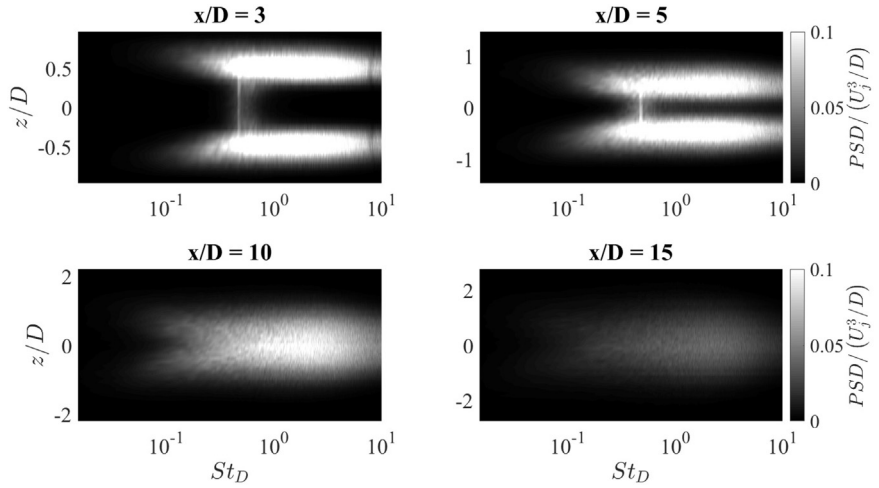

Fig. 7. Acceleration PSD map along the transverse direction z at different axial distances in free-jet conditions.

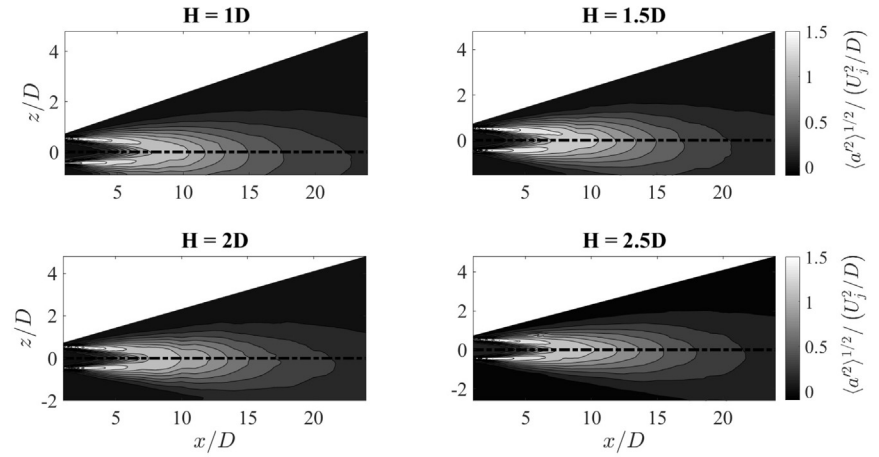

Fig. 8. Contour maps of the normalized acceleration standard deviation in the plane x–z for all the jet–plate configurations. Dash-dotted lines refer to the nozzle axis.

brings about local accelerations of the flow due to the injection of the ambient fluid in the jet. On the contrary, the negative skewness values define the potential core shape. Likewise, kurtosis exhibits large values associated with high-energy intermittency regions only in the shear layers, the amplitude being larger in the external shear layers. It is observed that the presence of the plate prevents the development of the shear layer in the jet region close to the surface, thus reducing the generation of intermittent events in such region.

4.2. Multi-variate statistics between acceleration and wall pressure

The cross-statistics between acceleration and wall pressure were achieved considering the HW probe and microphone at consecutive streamwise locations. Specifically, the acceleration signal at the ith axial position was correlated with the wall-pressure signal measured at the $(i+1)$th axial location.

Fig. 11 shows the contour maps of the streamwise evolution of the cross-correlation coefficient between acceleration and wall-pressure signals along the nozzle axis for all the jet–plate configurations. It is observed that significant correlation levels were found only for axial positions within the potential core, the correlation exhibiting an oscillatory shape that could be ascribed to the Kelvin–Helmholtz instability. Such an inference is further supported by the decrease of the correlation level for further jet–plate distances, the amplitude of the Kelvin–Helmholtz instability mode being characterized by an exponential decay along r [27].

The axial evolution of the cross-correlation coefficient between wall pressure and acceleration signals at the HW transverse position ζ for all the radial distances of the surface from the jet is shown in Fig. 12. It is noted that both correlation shape and amplitude depend on the jet–plate distance and the streamwise region of the jet considered, the larger correlation values being found for increasing axial distances as the flat plate was moved away from the jet. For $H/D = 1$, a narrow

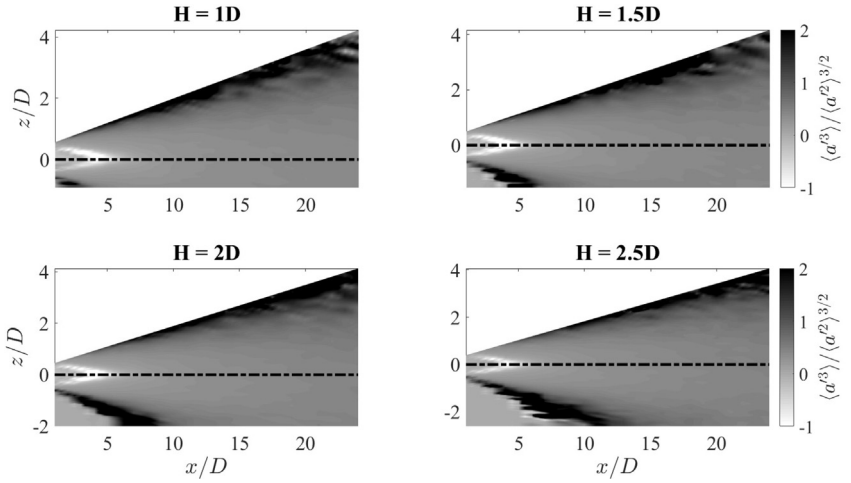

Fig. 9. Contour maps of the acceleration skewness factor in the plane x–z for all the jet–plate configurations. Dash-dotted lines refer to the nozzle axis.

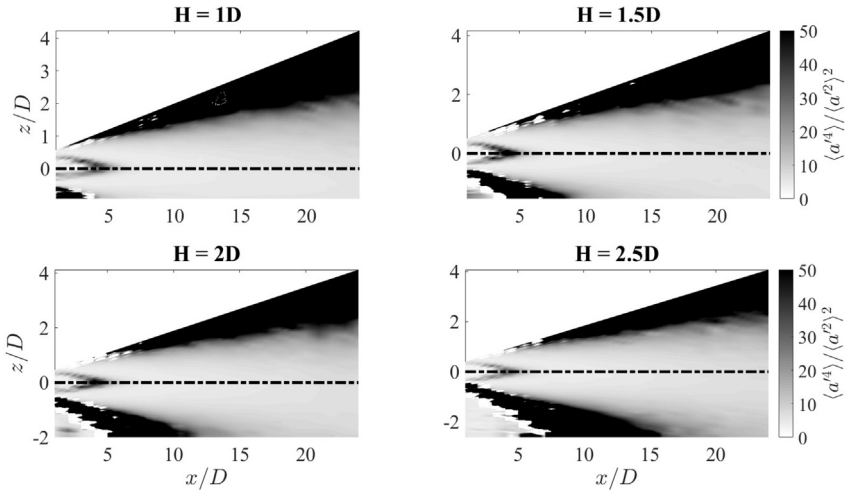

Fig. 10. Contour maps of the acceleration flatness factor in the plane x–z for all the jet–plate configurations. Dash-dotted lines refer to the nozzle axis.

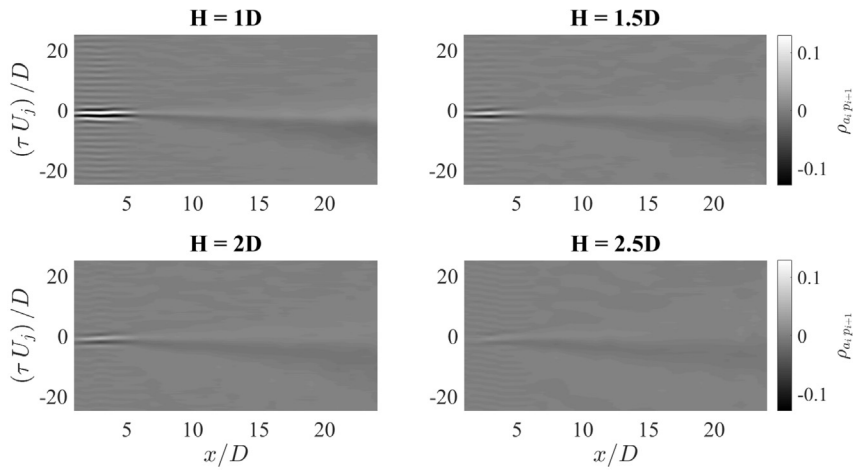

Fig. 11. Streamwise evolution of the cross-correlation coefficient between acceleration and wall-pressure signals along the nozzle axis for all the jet–plate configurations.

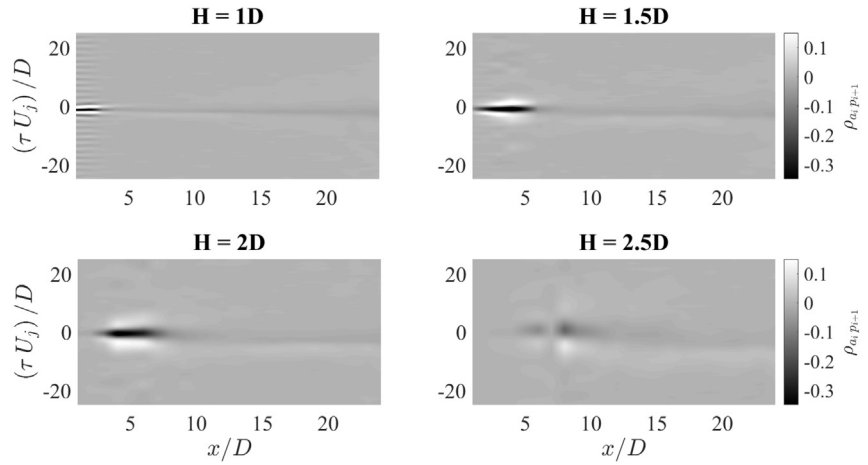

Fig. 12. Streamwise evolution of the cross-correlation coefficient between acceleration and wall-pressure signals at transverse position ζ for all the jet–plate configurations.

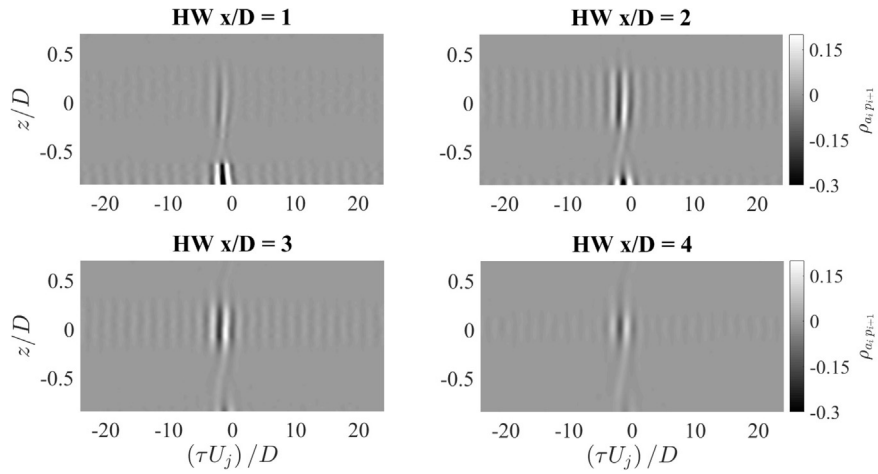

Fig. 13. Cross-wise evolution of the cross-correlation coefficient between acceleration and wall-pressure signals at HW axial positions upstream the jet impact point on the surface for the jet–plate configuration $H = 1\,D$.

oscillatory correlation shape was detected immediately downstream the nozzle exhaust. For further jet–surface distances the oscillations reduce and a dominant negative drop appears.

The evolution along the z-direction of the cross-correlation coefficient between acceleration and wall pressure is shown in Fig. 13. The jet–plate distance $H = 1D$ has been considered here as the configuration representative of the strongest jet–plate interaction. The stream-wise locations $x/D = 1$, 2, 3, and 4 upstream of the jet impact point on the surface were taken into account, the correlation levels being negligible for larger x/D, as shown in Figs. 11 and 12. Significant correlation levels were found for transverse positions in the core of the jet and close to the plate. The oscillations in the correlation exhibit a phase shift between the central and the outer z-locations of the jet. Indeed, for such transverse positions, the oscillations reduce with increasing x/D.

The dominance of the Kelvin–Helmholtz instability mode in the potential core is further highlighted in Fig. 14, which shows the dimensionless Cross-Power Spectral Density (CPSD) between the acceleration and wall-pressure signals along the z-direction at different axial distances. The cross-spectrum was normalized by dividing by the time scale D/U_j, the characteristic acceleration U_j^2/D and a reference pressure p_ref, whose value was set to 20 µPa, the resulting scaling parameter being $U_\mathrm{j}\,p_\mathrm{ref}$. For the sake of brevity, only the results concerning the plate radial distance $H = 1\,D$ were considered, the trend obtained being similar for the other jet–plate distances. It is observed that, for small axial distances within the potential core, a strong energy peak for $St_D \approx 0.47$ is clearly detected for almost all z-positions, its signature being stronger for transverse locations in the core of the jet. For axial positions further downstream in the jet plume, the spectral energy reduces significantly, its value being almost negligible.

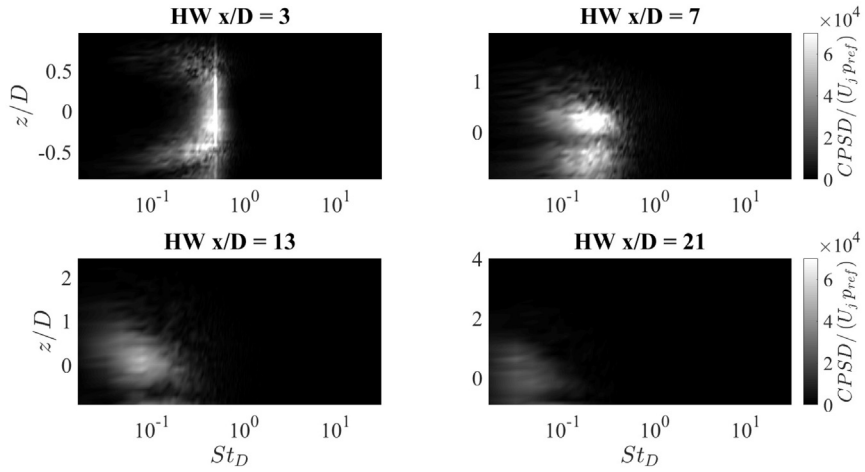

Fig. 14. Crosswise evolution of the normalized cross-spectra amplitude between acceleration and wall-pressure signals at different axial distances for the jet–plate configuration $H/D = 1$.

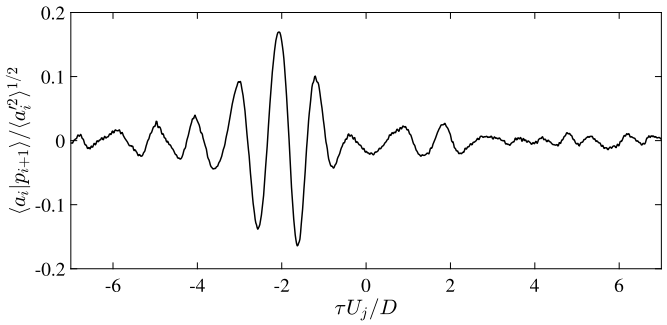

Fig. 15. Acceleration signature conditioned on wall pressure at HW axial position $x/D = 1$, transverse position $z/D \approx -0.6$ for the jet–plate configuration $H = 1D$. Wavelet scale/pseudo-frequency corresponds to $St_D \approx 0.47$, i.e. the one at which occurs the roll-up of the shear layer.

4.3. Signatures of acceleration conditioned on wall pressure

Previously to the presentation of the acceleration signatures, some of the peculiar features concerning the velocity signatures conditioned on the wall pressure events presented in Mancinelli et al. [10,11] are briefly recalled. Specifically, positive spike-shape velocity signatures related to coherent ring-like vortices convected by the mean flow were detected for axial positions downstream of the jet impact on the plate and for transverse positions close to the surface.

Indeed, the comparison of the outcome obtained between the velocity and the acceleration sheds light on the physics of the jet–plate interaction phenomena. The acceleration signatures reported hereinafter are represented in dimensionless form, the normalization being achieved by dividing by the local standard deviation of the conditioned time signal. For the sake of brevity, the plate positions $H/D = 1$ and 1.5 are considered, the acceleration signatures being noisier and less significant for the furthest jet–plate distances. Likewise the cross-statistical analysis, consecutive positions in the streamwise direction were considered for the HW and microphone probes in the conditional statistic analysis.

An example of the cross-conditioned acceleration signatures obtained for the jet–plate distance $H/D = 1$ at the HW axial and transverse locations equal to $x/D = 1$ and $z/D \approx -0.6$, respectively, is shown in Fig. 15. As recently performed by Camussi et al. [28], the wavelet scale/pseudo-frequency of the LIM of the wall-pressure signal here considered is the one corresponding to the characteristic Strouhal number of the roll-up of the shear layer, that is $St_D \approx 0.47$. The educed acceleration structure exhibits a dumped oscillatory signature, its phase speed based on the separation distance between the HW and microphone probes and the time delay of the ensemble average peak being of the order of the jet velocity ($\approx 0.5\,U_j$). On account of the features just described and of the outcome reported throughout the paper, it is reasonable to assert that the ensemble average educed by the wavelet-based approach is the signature of the Kelvin–Helmholtz hydrodynamic wavepacket [29].

It is interesting to point out that the shape of the educed signature does not significantly depend on the wavelet scale/frequency considered in the LIM of the wall-pressure signal, as highlighted in Fig. 16. It is observed that the amplitude of the educed signature reduces as the Strouhal number decreases so that no appreciable ensemble averages are detected for $St_D < 0.3$. Such a behaviour could be related to the time derivative operation performed on the velocity signal which, as underlined above, implies the enhancement of the high-frequency energy content, and to the poor resolution of

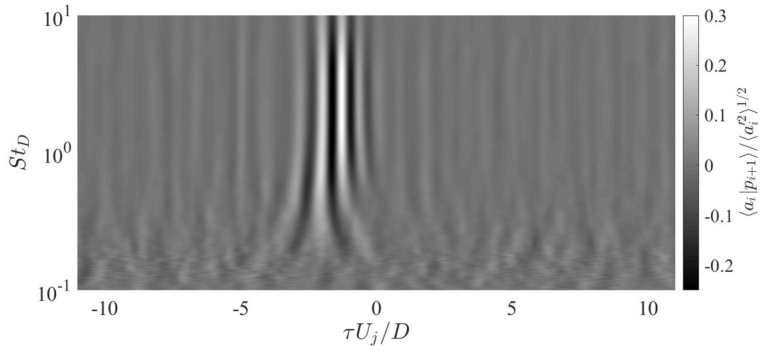

Fig. 16. Evolution along the wavelet scales/pseudo-frequencies of the acceleration signature conditioned on the wall pressure at HW axial position $x/D = 1$, transverse location $z/D \approx -0.6$ for the jet–plate distance $H/D = 1$.

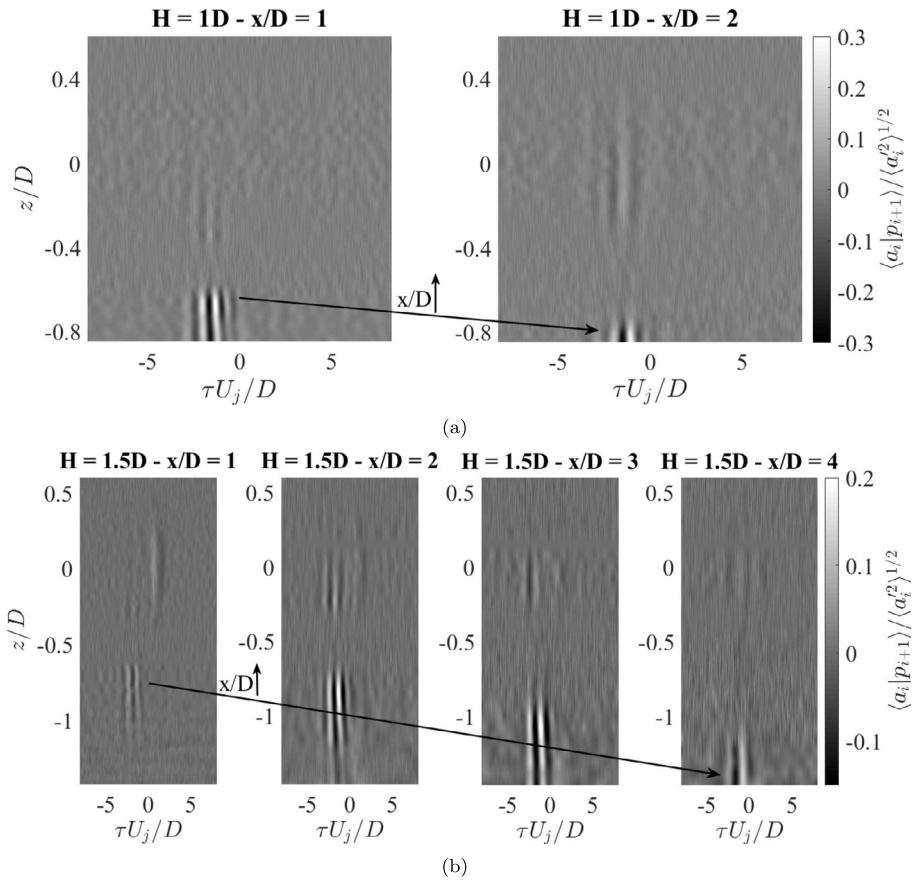

Fig. 17. Crosswise evolution of the normalized acceleration signatures at different axial distances for the jet–plate configurations: (a) $H/D = 1$, (b) $H/D = 1.5$.

the wavelet basis approaching the coarsest scales [30]. Indeed, as recently outlined by Sasaki et al. [31], the wavepacket signature in the jet flow can be found for high Strouhal numbers up to 4. It has to be pointed out that the characteristic time scale of the ensemble average enlarges as the frequency decreases, such a behaviour bringing about the reduction of the phase speed of the acceleration structure in agreement with previous results reported in the literature [32,33].

It has to be underlined that appreciable signatures were educed only for transverse positions in the proximity of the outer shear layer in the jet side region close to the surface. Furthermore, unlike the velocity, non-zero acceleration signatures were detected only for axial positions where the jet had not yet impinged on the plate. This result is clearly represented in Fig. 17, which shows the crosswise evolution along the z-direction of the extracted acceleration signatures at different axial distances and for both jet–plate distances $H/D = 1$, 1.5. For the sake of clarity of the representation, the LIM frequency at which the acceleration structure is computed is the one associated with the largest amplitude of the ensemble average,

that is $St_D \approx 1.9$. On account of the spreading of the jet in the streamwise direction, it is observed that the region where non-zero wavepacket signatures were educed was found at lower transverse positions z for increasing x/D, the associated structure being 'broken' as soon as the jet impinged on the plate. The pictures of the contour maps in the z–t domain of the extracted signatures appear as the snapshots of the same flow structure captured in its spatial evolution along the streamwise distance x, the spatial track of the flow signature in the x–z space being highlighted with an arrow.

5. Conclusions

In this paper, an experimental investigation of an incompressible jet interacting with a tangential flat plate at different radial distances from the nozzle axis was carried out. Simultaneous velocity and wall pressure measurements were performed by a hot-wire anemometer at different axial and transverse positions x and z and by a streamwise cavity-mounted microphone array, respectively. The analysis is the continuation of previous studies carried out by the same authors [9–11]. The objective of the present work was to characterize the cross- and conditioned statistics between acceleration and wall pressure fields. The local acceleration of the jet was estimated by the time derivative of the velocity signal measured by the HW anemometer.

A preliminary characterization of the acceleration field in free-jet conditions was provided in terms of statistical quantities and spectral content. To the best of the authors' knowledge, this was the first attempt to investigate experimentally the acceleration in the jet plume. As expected, the mean acceleration is zero for all the axial and radial locations in the jet. On the contrary, the fluctuating component is definitely more significant, its amplitude being close to 0 in the potential core and large in the proximity of the mixing layers and downstream of the potential core end. The evolution of the acceleration spectra along the nozzle axis underlined that the spectral energy was concentrated at middle-high frequencies, where a significant energy peak associated with the Kelvin–Helmholtz instability clearly appeared.

The effect of the plate on the acceleration field was quantified in terms of variation of the first-, third- and fourth-order statistical moments in the plane x–z. The bending of the jet due to the Coanda effect emerged in the contour maps of the acceleration standard deviation. The skewness and flatness factors highlighted that the plate had the effect to prevent the development of the external shear layer in the jet side close to the surface, thus reducing the generation of high-energy intermittent events.

The trend of the cross-correlation between acceleration and wall-pressure signals was found to be dependent on the jet–plate distance and on the probes spatial location in the plane x–z. On the transverse locations corresponding to the nozzle axis, significant correlation levels were found for axial positions within the potential core, the oscillatory correlation shape being associated with the Kelvin–Helmholtz instability. As the jet–plate distance increased, the correlation amplitude lowered according to the decrease of the Kelvin–Helmholtz mode amplitude with the increasing radial distance from the jet. For HW transverse positions closer to the plate, the correlation oscillations reduced, exhibiting a dominant negative peak. The dominance of the Kelvin–Helmholtz instability was further confirmed by the trend of the cross-spectra.

A cross-conditioning procedure based on wavelet transform was applied in order to educe the acceleration structures related to the energetic wall-pressure events. The outcome was compared with the one obtained in previous works by the same authors (see Mancinelli et al. [10,11]) considering the velocity signals. Velocity signatures were detected only for axial positions downstream of the jet impact on the plate and for transverse positions close to the surface, their positive spike shape being associated with a ring-like vortex structure. On the contrary, acceleration signatures were found for axial positions before the impingement of the jet on the plate and for transverse positions in the proximity of the external shear layer. The dumped oscillatory shape of the signature was related to a wavepacket structure convected by the flow, the educed structure being 'destroyed' as soon as the jet impinged on the plate.

Future developments of the present work could concern the evaluation of the velocity gradient through parallel double-component HW or PIV measurements in order to get an estimation of the convective term of the velocity derivative. It is authors' opinion that the multi-variate and conditioned statistics between acceleration and near-field pressure can provide a deeper insight on the jet noise generation mechanism in isolated as well as installed configurations, especially if the decomposition of the near pressure field into its hydrodynamic and acoustic components is achieved (see Mancinelli et al. [34,13,35]).

Acknowledgements

The authors acknowledge the partial support of the EU collaborative project JERONIMO (ACP2-GA-2012-314692) funded under the 7th Framework Program.

The authors would like to express their gratitude to the reviewers for the helpful comments and suggestions that allowed them to further improve the quality of the manuscript.

References

[1] J. Huber, M. Omais, A. Vuillemin, R. Davy, Characterization of installation effects for HBPR engine part IV: assessment of jet acoustics, in: 15th AIAA/CEAS Aeroacoustics Conference, AIAA Paper 2009-3371, American Institute of Aeronautics and Astronautics, 2009.

[2] J. Huber, G. Drochon, A. Pintado-Peno, F. Cléro, G. Bodard, Large-scale jet noise testing, reduction and methods validation EXEJET: 1. project overview and focus on installation, in: 20th AIAA/CEAS Aeroacoustics Conference, AIAA Paper 2014-3032, American Institute of Aeronautics and Astronautics, 2014.
[3] D. Papamoschou, S. Mayoral, Experiments on shielding of jet noise by airframe surfaces, in: 15th AIAA/CEAS Aeroacoustics Conference, AIAA Paper 2009-3326, American Institute of Aeronautics and Astronautics, 2009.
[4] G.G. Podboy, Jet-surface interaction test: phased array noise source localization results, in: ASME Turbo Expo 2012: Turbine Technical Conference and Exposition, American Society of Mechanical Engineers, 2012, pp. 381–414.
[5] A.V.G. Cavalieri, P. Jordan, W.R. Wolf, Y. Gervais, Scattering of wavepackets by a flat plate in the vicinity of a turbulent jet, J. Sound Vib. 333 (24) (2014) 6516–6531.
[6] S. Piantanida, V. Jaunet, J. Huber, W.R. Wolf, P. Jordan, A.V.G. Cavalieri, Scattering of turbulent-jet wavepackets by a swept trailing edge, J. Acoust. Soc. Am. 140 (6) (2016) 4350–4359.
[7] J. Vera, J.L.T. Lawrence, R.H. Self, M. Kingan, The prediction of the radiated pressure spectrum produced by jet-wing interaction, in: 21st AIAA/CEAS Aeroacoustics Conference, AIAA Paper 2015-2216, American Institute of Aeronautics and Astronautics, 2015.
[8] A. Di Marco, R. Camussi, M. Bernardini, S. Pirozzoli, Wall pressure coherence in supersonic turbulent boundary layers, J. Fluid Mech. 732 (2013) 445–456.
[9] A. Di Marco, M. Mancinelli, R. Camussi, Pressure and velocity measurements of an incompressible moderate Reynolds number jet interacting with a tangential flat plate, J. Fluid Mech. 770 (2015) 247–272.
[10] M. Mancinelli, A. Di Marco, R. Camussi, Cross-statistical and wavelet analysis of velocity and wall-pressure fields in jet-surface interaction, in: 22nd AIAA/CEAS Aeroacoustics Conference, AIAA Paper 2016-2861, American Institute of Aeronautics and Astronautics, 2016.
[11] M. Mancinelli, A. Di Marco, R. Camussi, Multi-variate and conditioned statistics of velocity and wall pressure fluctuations induced by a jet interacting with a flat-plate, J. Fluid Mech. 823 (2017) 134–165.
[12] K. Hanjalić, R. Mullyadzhanov, On spatial segregation of vortices and pressure eddies in a confined slot jet, Phys. Fluids 27 (3) (2015) 031703.
[13] M. Mancinelli, T. Pagliaroli, A. Di Marco, R. Camussi, T. Castelain, Wavelet decomposition of hydrodynamic and acoustic pressures in the near field of the jet, J. Fluid Mech. 813 (2017) 716–749.
[14] R. Camussi, S. Grizzi, Statistical analysis of the pressure field in the near region of a $M = 0.5$ circular jet, Int. J. Aeroacoust. 13 (1–2) (2014) 169–181.
[15] L. Chatellier, J. Fitzpatrick, Spatio-temporal correlation analysis of turbulent flows using global and single-point measurements, Exp. Fluids 38 (5) (2005) 563–575.
[16] C. Bogey, O. Marsden, C. Bailly, Effects of moderate Reynolds numbers on subsonic round jets with highly disturbed nozzle-exit boundary layers, Phys. Fluids 24 (10) (2012) 105107.
[17] K.B.M.Q. Zaman, Effect of initial boundary-layer state on subsonic jet noise, AIAA J. 50 (8) (2012) 1784–1795.
[18] C. Bogey, O. Marsden, C. Bailly, Large-eddy simulation of the flow and acoustic fields of a Reynolds number 10^5 subsonic jet with tripped exit boundary layers, Phys. Fluids 23 (3) (2011) 035104.
[19] R. Camussi, G. Guj, Experimental analysis of intermittent coherent structures in the near field of a high Re turbulent jet flow, Phys. Fluids 11 (2) (1999) 423–431.
[20] C. Torrence, G.P. Compo, A practical guide to wavelet analysis, Bull. Am. Meteorol. Soc. 79 (1) (1998) 61–78.
[21] M. Farge, Wavelet transforms and their applications to turbulence, Annu. Rev. Fluid Mech. 24 (1) (1992) 395–458.
[22] S.D. Meyers, B.G. Kelly, J.J. O'Brien, An introduction to wavelet analysis in oceanography and meteorology: with application to the dispersion of Yanai waves, Mon. Weather Rev. 121 (10) (1993) 2858–2866.
[23] C. Meneveau, Analysis of turbulence in the orthonormal wavelet representation, J. Fluid Mech. 232 (1991) 469–520.
[24] R. Camussi, J. Grilliat, G. Caputi-Gennaro, M.C. Jacob, Experimental study of a tip leakage flow: wavelet analysis of pressure fluctuations, J. Fluid Mech. 660 (2010) 87–113.
[25] T. Pagliaroli, M. Mancinelli, G. Troiani, U. Iemma, R. Camussi, Fourier and wavelet analyses of intermittent and resonant pressure components in a slot burner, J. Sound Vib. 413 (2018) 205–224.
[26] R. Camussi, G. Guj, Orthonormal wavelet decomposition of turbulent flows: intermittency and coherent structures, J. Fluid Mech. 348 (1997) 177–199.
[27] T. Suzuki, T. Colonius, Instability waves in a subsonic round jet detected using a near-field phased microphone array, J. Fluid Mech. 565 (2006) 197–226.
[28] R. Camussi, M. Mancinelli, A. Di Marco, Intermittency and stochastic modeling of hydrodynamic pressure fluctuations in the near field of compressible jets, Int. J. Heat Fluid Flow 68 (2017) 180–188.
[29] A.V.G. Cavalieri, P. Jordan, A. Agarwal, Y. Gervais, Jittering wave-packet models for subsonic jet noise, J. Sound Vib. 330 (18) (2011) 4474–4492.
[30] M. Farge, K. Schneider, O. Pannekoucke, R. Nguyen Van Yen, Multiscale representations: fractals, self-similar random processes and wavelets, in: Handbook of Environmental Fluid Dynamics, vol. 2, CRC Press, 2012, chapter 23.
[31] K. Sasaki, A.V.G. Cavalieri, P. Jordan, O.T. Schmidt, T. Colonius, G.A. Brès, High-frequency wavepackets in turbulent jets, J. Fluid Mech. 830 (2017).
[32] P.J. Morris, K.B.M.Q. Zaman, Velocity measurements in jets with application to noise source modeling, J. Sound Vib. 329 (4) (2010) 394–414.
[33] V. Jaunet, P. Jordan, A.V.G. Cavalieri, Two-point coherence of wave packets in turbulent jets, Phys. Rev. Fluids 2 (2) (2017) 024604.
[34] M. Mancinelli, T. Pagliaroli, A. Di Marco, R. Camussi, T. Castelain, O. Léon, Hydrodynamic and acoustic wavelet-based separation of the near-field pressure of a compressible jet, in: 22nd AIAA/CEAS Aeroacoustics Conference, Lyon, France, 30 May–1 June 2016, AIAA Paper 2016-2864, American Institute of Aeronautics and Astronautics, 2016.
[35] M. Mancinelli, T. Pagliaroli, R. Camussi, T. Castelain, On the hydrodynamic and acoustic nature of pressure proper orthogonal decomposition modes in the near field of a compressible jet, J. Fluid Mech. 836 (2018) 998–1008.